Design and analysis of transmission enhanced multi-segment grating in MZI configuration for slow light applications

Shengling Deng and Z. Rena Huang*

Department of Electrical, Computer, and System Engineering, Rensselaer Polytechnic Institute, 110 8th St, Troy, New York 12180, USA

*huangz3@rpi.edu

Abstract: This paper proposes to use slow light effects near the Brillouin zone band edge of one-dimensional gratings for reducing the size of integrated electro-optic (EO) modulators. The gratings are built within the arms of a Mach-Zehnder Interferometer (MZI) for intensity modulation. To overcome the inherent high reflection and low extinction ratio, we introduce various multi-segment grating designs. We use coupled-mode theory and derive transfer matrices to analyze the spectral transmittance and phase delay of each arm of the interferometer. Calculations show that a size-reduction of a factor of 2 or more can be achieved at $\lambda = 1.574\mu m$ with an insertion loss of 0.17dB and an amplitude modulation extinction ratio of 18.84dB. The simulated structure is based on a Si slab-waveguide 0.2 μm thick with 30nm deep grating groves on SiO_2 substrate.

OCIS codes: (130.2790) Guided waves; (050.2770) Gratings; (130.3120) Integrated optics devices; (230.1480) Bragg reflectors.

References and links

1. A. Liu, R. Jones, L. Liao, D. Samara-Rubio, D. Rubin, O. Cohen, R. Nicolaescu, and M. Paniccia, "A high-speed silicon optical modulator based on a metal-oxide-semiconductor capacitor," Nature **427**(6975), 615–618 (2004).
2. Y. Jiang, W. Jiang, L. Gu, X. Chen, and R. T. Chen, "80-micron interaction length silicon photonic crystal waveguide modulator," Appl. Phys. Lett. **87**(22), 221105 (2005).
3. A. Liu, L. Liao, D. Rubin, H. Nguyen, B. Ciftcioglu, Y. Chetrit, N. Izhaky, and M. Paniccia, "High-speed optical modulation based on carrier depletion in a silicon waveguide," Opt. Express **15**(2), 660–668 (2007).
4. E. F. Schipper, A. M. Brugman, C. Dominguez, L. M. Lechuga, R. P. H. Kooyman, and J. Greve, "The realization of an integrated Mach-Zehnder waveguide immunosensor in silicon technology," Sens. Actuators B Chem. **40**(2-3), 147–153 (1997).
5. B. J. Luff, J. S. Wilkinson, J. Piehler, U. Hollenbach, J. Ingenhoff, and N. Fabricius, "Integrated optical Mach–Zehnder biosensor," J. Lightwave Technol. **16**(4), 583–592 (1998).
6. S. Deng, Z. R. Huang, and J. F. McDonald, "Design of high efficiency multi-GHz SiGe HBT electro-optic modulator," Opt. Express **17**(16), 13425–13428 (2009).
7. T. F. Krauss, "Slow light in photonic crystal waveguides," J. Phys. D Appl. Phys. **40**(9), 2666–2670 (2007).
8. M. L. Povinelli, S. G. Johnson, and J. D. Joannopoulos, "Slow-light, band-edge waveguides for tunable time delays," Opt. Express **13**(18), 7145–7159 (2005).
9. C. Monat, B. Corcoran, D. Pudo, M. Ebnali-Heidari, C. Grillet, M. D. Pelusi, D. J. Moss, B. J. Eggleton, T. P. White, L. O'Faolain, and T. F. Krauss, "Slow Light Enhanced Nonlinear Optics in Silicon Photonic Crystal Waveguides," IEEE J. Sel. Top. Quantum Electron. **16**(1), 344–356 (2010).
10. J. F. McMillan, X. Yang, N. C. Panoiu, R. M. Osgood, and C.-W. Wong, "Enhanced stimulated Raman scattering in slow-light photonic crystal waveguides," Opt. Lett. **31**(9), 1235–1237 (2006).
11. M. Soljačić, S. G. Johnson, S. Fan, M. Ibanescu, E. Ippen, and J. D. Joannopoulos, "Photonic-crystal slow-light enhancement of nonlinear phase sensitivity," J. Opt. Soc. Am. B **19**(9), 2052–2059 (2002).
12. D. J. Moss, B. Corcoran, C. Monat, C. Grillet, T. P. White, L. O'Faolain, T. F. Krauss, and B. J. Eggleton, "Slow-light enhanced nonlinear optics in silicon photonic crystal waveguides," PIER **6**, 273–278 (2010).
13. L. Wei, and J. Lit, "Phase-shifted Bragg grating filters with symmetrical structures," J. Lightwave Technol. **15**(8), 1405–1410 (1997).
14. M. Yamada, and K. Sakuda, "Analysis of almost-periodic distributed feedback slab waveguides via a fundamental matrix approach," Appl. Opt. **26**(16), 3474–3478 (1987).

#137559 - $15.00 USD Received 2 Nov 2010; revised 11 Mar 2011; accepted 29 Mar 2011; published 8 Apr 2011

15. G. P. Agrawal, and S. Radic, "Phase-shifted fiber Bragg grating and their application for wavelength demultiplexing," IEEE Photon. Technol. Lett. **6**(8), 995–997 (1994).
16. Y. A. Vlasov, and S. J. McNab, "Coupling into the slow light mode in slab-type photonic crystal waveguides," Opt. Lett. **31**(1), 50–52 (2006).
17. M. Nevière, and E. Popov, *Light propagation in periodic media: differential theory and design*, (CRC Press, 2002).
18. S.-L. Chuang, *Physics of optoelectronic devices*, (John Wiley & Sons, Inc, 1995), chap. 8.
19. M. V. Klein, and T. E. Furtak, *Optics*, (John Wiley & Sons, Inc, 1986), chap.5.

1. Introduction

Numerous photonic devices utilize integrated Mach-Zehnder interferometer (MZI) to achieve phase-to-intensity conversion, such as electro-optic (EO) modulators [1–3] and bio-sensors [4,5]. For a fixed voltage swing, the waveguide length L_π for which a π phase-difference occurs between the two MZI arms can be used to characterize the device efficiency [6]. Incorporation of slow light effects in the MZI is a practical and effective way to improve device efficiency and reduce power consumption. The slow light effect has been widely investigated in two-dimensional (2D) photonic crystal (PhC) waveguides in the past few years [7–12]. An EO modulator utilizing slow light effect, having L_π = 80μm, was demonstrated by forming a 2D PhC waveguide with a defect structure [2].

A slab waveguide with a periodic grating structure is a one-dimensional (1D) PhC. This differs from a PhC waveguide with light propagating at its defect mode, in that slow light propagation occurs in 1D gratings when the wavelength is near the Brillouin band edge. The 1D grating presents an alternative approach for reducing the EO modulator size. In this paper, we use coupled-mode theory to obtain detailed expressions for the dispersion relation and the transmission spectrum of a 1D grating. Finally we discuss the operation of the MZI EO modulator and show expressions for the arm length reduction.

A major challenge of the 1D grating is that high transmittance is not always obtainable simultaneously with the onset of slow light. In the MZI configuration, the problem becomes even more severe as each arm is expected to transport the same optical power with minimal insertion loss. To achieve these two conditions, we propose and investigate a multi-segment grating design. The multi-segment structure is formed by placing a plain slab waveguide between two grating segments. The purpose of the plain slabs is to form a Fabry-Perot cavity between the two grating segments. We use coupled-mode theory to obtain transfer matrices so as to describe the behavior of slow light propagating in this new structure. A similar approach was used to calculate the transmission and reflection characteristics of phase-shifted gratings [13–15]. In this work, we investigate enhancement of the slow light transmittance, and the behavior of phase delay, as a function of grating spacer length. We further point out the trade-offs between grating design and performance. When the MZI arm length is reduced by a factor of 2 to 3, the group index of the structure is in the range $n_g < 5$. The advantage of a slow light waveguide with a relatively small group index is that it minimizes the coupling loss caused by impedance mismatch [16].

2. Device structures

A sketch of the grating arm MZI is shown in Fig. 1(a). The 1D periodic grating can be fabricated by reactive ion etching. We consider only TE-polarized light propagating in the *z*-direction of a symmetric $SiO_2/Si/SiO_2$ slab-waveguide, as shown in Fig. 1(b) where n_1 and n_2 are the real parts of the indices of refraction of Si and SiO_2, respectively, and **a** and **Λ** are the groove depth and grating pitch, respectively. The transmitted and the reflected fields are shown in Fig. 1(c) for light incident from left and are represented by **A** and **B** at the respective boundaries at z = 0 and z = L. Only first order diffraction is considered.

A phase difference $\Delta\varphi$ between the two arms is introduced by a change Δn in the refractive index of one of the arms. In the case of slow light propagation, a given value of $\Delta\varphi$ is obtained in a shorter propagation distance simply because of the larger effective index represented by

#137559 - $15.00 USD Received 2 Nov 2010; revised 11 Mar 2011; accepted 29 Mar 2011; published 8 Apr 2011

the propagation constant difference between the two arms, Δβ. The larger the real value of β, the slower the propagation group speed of light. We explore slow light propagation in a semiconductor grating structure for light energy near the Brillouin zone boundary of the 1D periodic structure.

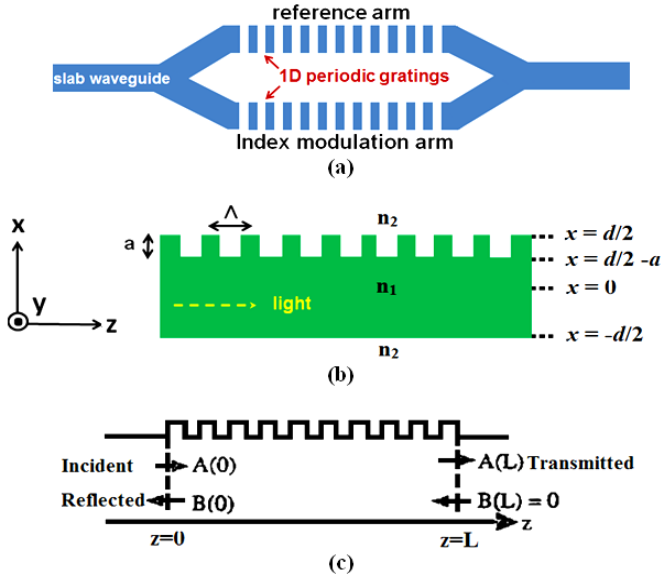

Fig. 1. (a) A 1D grating incorporated in a MZI configuration, (b) symmetric slab waveguide with 1D grating on one surface, and (c) illustration of steady-state fields.

The grating period Λ for the grating structure satisfies the Bragg condition $\Lambda = 2\lambda_0/N_{eff}$, where N_{eff} is the real part of the effective index of the waveguide, and λ_0 is the incident wavelength in vacuum. The groove width is half of the grating period. The groove depth and profile are two important parameters in a grating design, as will be discussed in detail below.

3. Dispersion and spectral transmission

Coupled-mode theory is widely used in analyzing mode coupling in parallel waveguides and grating structures. In the case of a 1D grating, mode coupling occurs between forward and backward-traveling waves. For a multi-mode waveguide, because higher order modes are often truncated in numerical calculations, both spectral dispersion and transmission spectra obtained by coupled-mode theory, are approximate [17].

As light propagates along a periodic grating, partial reflection occurs at each groove which represents an abrupt discontinuity. At the Bragg condition, the forward- and backward-propagating waves are in-phase so the coupling gives rise to a standing-wave. For wavelengths near the Bragg condition, the forward- and backward-waves are slightly out of phase, leading to a slow-moving traveling wave interference pattern. When this happens, a stop-band or gap develops in the transmission spectrum. In momentum space, or *k*-space, the slow mode occurs when the propagation constant is close to the Brillouin zone boundary. Because slow light effects occur only near the Brillouin zone band edge for a 1D grating, the spectral bandwidth is limited.

The real part of the dielectric constant, ε_r, can be written as $\varepsilon_r(x,z) = \varepsilon_r^{(0)}(x,z) + \Delta\varepsilon_r(x,z)$, where $\varepsilon_r^{(0)}(x,z)$ is the index of refraction of the bulk semiconductor silicon, and $\Delta\varepsilon_r$ is the periodic index perturbation. As a periodic function, $\Delta\varepsilon_r$ can be expanded in a Fourier sum of odd harmonics. According to coupled-mode theory, the electric-field component E_y is expanded in terms of all modes supported by the unperturbed waveguide. Expressions of $\Delta\varepsilon_r$ and E_y are shown in Eq. (1) as

#137559 - $15.00 USD Received 2 Nov 2010; revised 11 Mar 2011; accepted 29 Mar 2011; published 8 Apr 2011

$$\begin{cases} \Delta\varepsilon_r(x,z) = \sum_{p=-\infty}^{\infty} d_p(x) e^{ip\frac{2\pi}{\Lambda}z}, \\ E_y(x,z) = \sum_{m=-\infty}^{\infty} A_m(z) E_y^{(m)}(x) e^{i\beta_m z}, \end{cases} \tag{1}$$

where $E_y^{(m)}$ is the m^{th}-order unperturbed mode, and β_m is the corresponding propagation constant.

Considering only the 1st diffraction order (p = 1) and the fundamental mode of the optical waveguide, the effective propagation constant β_c and dispersion relation of a 1D grating are shown in Eqs. (2) and (3), where $|K|$ denotes the magnitude of coupling coefficient [18].

$$\beta_C = \frac{\pi}{\Lambda} \pm \sqrt{\left[\left(\beta_1(\omega)\right) - \left(\frac{\pi}{\Lambda}\right)\right]^2 - |K|^2}, \tag{2}$$

$$|K| = \frac{\omega}{4}\left|\int_{-\infty}^{\infty} d_\ell(x)\left|E_y^{(s)}(x)\right|^2 dx\right|. \tag{3}$$

The two solutions of β_C correspond to the two system modes in the grating. To obtain the complete dependence of β_C on ω, $|K|$ and the fundamental mode propagation constant β_1, Eqs. (2) and (3) are to be solved simultaneously for each frequency ω. Since the mathematical representation for $\Delta\varepsilon_r(x,z)$ depends on geometric details, $|K|$ differs from one groove profile to another. The expressions of $|K|$ for rectangular- and triangular-groove are obtained, for example, in Eq. (4):

$$|K| = \begin{cases} \left|\frac{\omega\varepsilon_0}{4\pi}\left(n_2^2 - n_1^2\right)\int_{\frac{d}{2}-a}^{\frac{d}{2}}\left|E_y^{(1)}(x)\right|^2 dx\right|, & \text{(rectangular)} \\ \left|\frac{\omega\varepsilon_0}{4\pi}\left(n_2^2 - n_1^2\right)\int_{d/2-a}^{d/2}\cos\left[\frac{\pi}{2a}\left(x-\frac{d}{2}\right)\right]\left|E_y^{(1)}\right|^2 dx\right|. & \text{(triangular)} \end{cases} \tag{4}$$

Since a cosine function appears in the integration of $|K|$ for triangular grooves, the coupling strength is weaker in the case of triangular grooves. The transmission spectrum of 1D grating with rectangular grooves is shown in Eq. (5) [18], where L is the grating length and $\delta\beta$ is defined as $\beta_1 - \pi/\Lambda$:

$$|t(L)|^2 = \frac{1 - \left(\frac{\delta\beta}{|K|}\right)^2}{\left(\frac{\delta\beta}{|K|}\right)^2 \left(\sinh(SL)\right)^2 + \left(1 - \left(\frac{\delta\beta}{|K|}\right)^2\right)\left(\cosh(SL)\right)^2}. \tag{5}$$

3.1 Transmittance

The transmission spectrum of a grating structure is determined by groove depth and grating length, (expressed as the number of grating periods). A $SiO_2/Si/SiO_2$ symmetric slab-waveguide with a core thickness of 0.2μm is considered in this work. The refractive index of the core is taken as n_c = 3.42, and that of the top and bottom cladding indices as n_2 = 1.45. The period of the 1st order grating is Λ = 0.2851μm for an incident vacuum wavelength λ_0 = 1.55μm.

The transmission spectrum for groove depth of 10nm, 20nm, and 30nm are calculated from Eq. (5) and graphically displayed in Fig. 2 (a). It is clear that the groove depth and its control during fabrication strongly affects the grating transmittance and can be used to obtain the desired transmittance value.

#137559 - $15.00 USD Received 2 Nov 2010; revised 11 Mar 2011; accepted 29 Mar 2011; published 8 Apr 2011

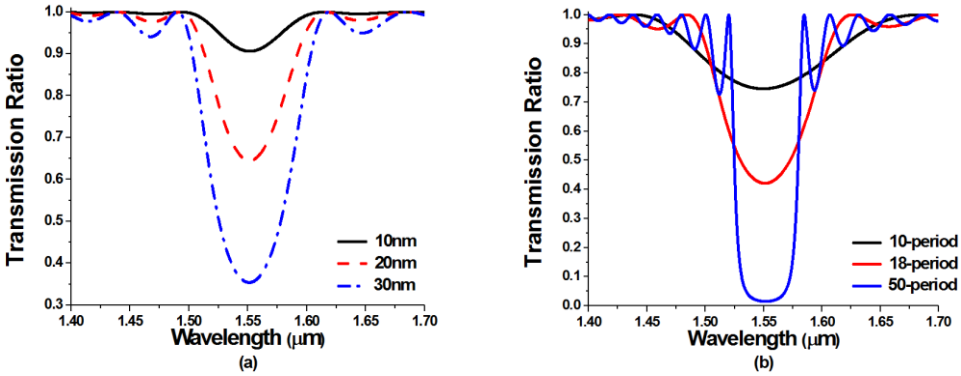

Fig. 2. Transmittance for (a) a 20-period rectangular grating for three groove depths, and (b) a grating with 30nm-deep grooves but having different numbers of periods.

The effective attenuation distance L_p can be used to describe how far a lightwave at a particular vacuum wavelength propagates into the grating waveguide. It is a useful measure for evaluating the relation between transmittance and grating length. L_p is mathematically defined by $\exp(-z\beta_{Cimg})$ as the distance into the grating at which the optical power has decayed to 1/e of the incident value. Thus, $L_p = 1/\beta_{Cimg}$, where β_{Cimg} is the imaginary part of β_C. From the above equations we find an attenuation distance $L_p = 5.14\mu m$ when light of vacuum wavelength $\lambda_0 = 1.55\mu m$ propagates in a silicon slab grating having groove depth of 30nm. This attenuation length corresponds to a grating with 18 periods (18Λ). Transmittances for gratings with periods 10Λ, 18Λ, and 50Λ are obtained from Eq. (5) and are plotted in Fig. 2(b). Near the Bragg wavelength, the transmittance decreases as the number of grating periods increases until a stopband forms as is the case of the 50-period (50Λ)-grating. Further increasing the number of periods leads to broadening of the stop-band. It can be inferred from the discussion that a 1D grating is subject to a length-constraint if a certain value of transmittance is expected.

3.2 Dispersion relation

The normalized dispersion relation for grating depth of 10nm, 20nm, and 30nm is plotted in Fig. 3 for the real part of the propagation constant β_C. Mode propagation direction can be determined from the sign of group velocity $v_g = d\omega/d\beta_C$. As is indicated in Fig. 3, deeper grooves lead to a wider bandgap, owning to stronger light scattering from deeper grooves. It is also seen that deeper grooves exhibit larger radii of curvature near the Brillouin zone edge or band edge, where $d\omega/d\beta_C$ is smaller, indicating a lower group velocity.

#137559 - $15.00 USD Received 2 Nov 2010; revised 11 Mar 2011; accepted 29 Mar 2011; published 8 Apr 2011

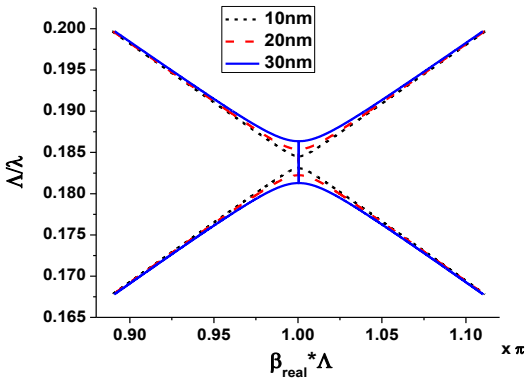

Fig. 3. Dispersion relations for rectangular grating grooves of different depths.

The effects of groove profiles on β_C are shown in Fig. 4, where only the forward mode is plotted. The dispersion relations reveal a wider bandgap and a greater $|\beta_{Cimg}|$ for the rectangular groove as a result of larger coupling coefficient $|K|$. When a refractive index change Δn occurs in the waveguide core, the dispersion relation shifts accordingly as a result of a detuned Bragg wavelength. When $\Delta n = 0$, $\Delta n = -0.01$, the two corresponding dispersion curves for triangular and rectangular grating of 30 nm depth are shown in Fig. 4.

Due to the irregular dispersion characteristics near the band edge, it is possible to obtain a larger $\Delta\beta$ at the Brillouin zone edge, as shown in Fig. 4(a) where it can also be seen that $\Delta\beta_{Creal}(\omega)$ depends strongly on ω and approaches $\Delta\beta$ in slab-waveguides as ω moves away from band edge.

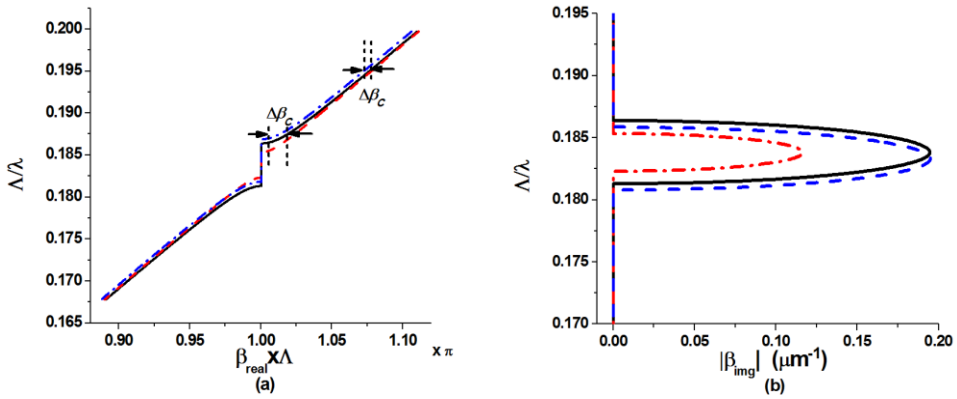

Fig. 4. Dispersion relation of (a) β_{Creal} (b) $|\beta_{Cimg}|$ for rectangular grating (solid) and triangular grating (dash-dot) at $\Delta n = 0$, and rectangular grating (dash) at $\Delta n = -0.01$.

4. MZI length reduction utilizing slow light effect

For devices based on MZI, $\Delta\varphi$ is converted into intensity modulation through interference at the output. The best extinction ratio is achieved by comparing the transmitted amplitudes when $\Delta\varphi = 0$ and $\Delta\varphi = \pi$. In the following calculations, a relatively large and uniform Δn of -0.01 is assumed in the modulation arm. The large Δn allows the device to be a few tens of microns, and display a relatively narrow stop band, however, the grating cannot be too long because of the finite propagation length.

#137559 - $15.00 USD Received 2 Nov 2010; revised 11 Mar 2011; accepted 29 Mar 2011; published 8 Apr 2011

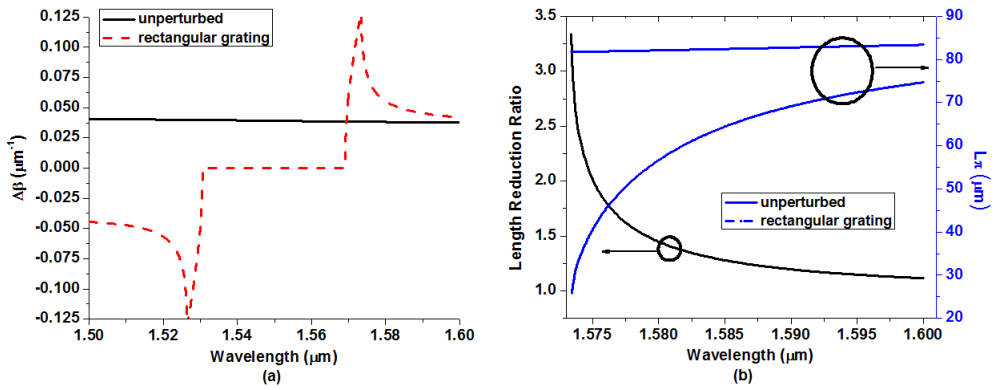

Fig. 5. (a) $\Delta\beta$ for a waveguide slab with and without gratings (b) L_π and length reduction ratio for a slab waveguide with rectangular grating grooves 30nm deep, as compared to a planar slab waveguide.

The length reduction effect is easier to understand from the viewpoint of $\Delta\beta_C$. The wavelength dependence of $\Delta\beta_C$ is shown in Fig. 5(a), which is obtained by measuring the dispersion shift in Fig. 4(a) at each wavelength. The singularities in Fig. 5(b) are the result of the finite number of data points in the numerical computation. It is seen from Fig. 5(a) that $\Delta\beta_C$ is about 0.122μm^{-1} at λ = 1.573μm for a grating with rectangular grooves 30nm deep. For the unperturbed slab-waveguide, $\Delta\beta$ is about 0.0385μm^{-1}. Therefore, a silicon grating with rectangular grooves reduces L_π by a factor of 3, when compared to a plane slab waveguide, as estimated from $L_\pi = \pi/\Delta\beta_C$. Further calculations also show that a length reduction of 3 still holds for a MZI with a Δn of the order of −0.001. Of course, smaller Δn values generally result in overall longer L_π.

Based on the $\Delta\beta$ calculation results shown in Fig. 5(a), the π phase shift length L_π is calculated and shown in Fig. 5(b). Since $|\Delta\beta_C|$ is symmetric in wavelength, only those wavelengths longer than Bragg wavelength are plotted in Fig. 5(b). The length reduction ratio is defined as L_π(slab)/L_π(rectangular) and is also shown in Fig. 5(b). L_π (slab) refers to the silicon slab waveguide and L_π (rectangular) to the silicon slab waveguide with one surface structured with a rectangular groove grating. It is evident that the reduction ratio degrades rapidly as the wavelength moves away from the band edge, and thus only a narrow wavelength range offers significant length reduction.

5. MZI with a multi-segment grating structure

As shown in Fig. 5(b), each length reduction-ratio corresponds to a particular operating wavelength. The transmission spectrum oscillates drastically with wavelength in the slow light region, while the transmittance for a particular wavelength is strongly affected by the grating length. As a result, the transmittance for a specific wavelength can be very low, leading to a high insertion loss for the corresponding reduction ratios. Additionally, as a refractive index shift is introduced in the modulation arm of the MZI, the transmittance between the modulation arm and the reference arm can differ by a large value. Exceptions occur at certain wavelengths, for which the transmittance of the modulation arm and the reference arm happen to be large simultaneously. However, in general, low insertion loss and high extinction ratio are not simultaneously attainable in a MZI having a uniform or single grating waveguide in each branch. To address this problem, we propose the multi-segment grating design that incorporates a number of equal-length grating segments and spacers, as sketched in Fig. 6.

Let's take the simplest two-segment configuration (M = 2) as an example. The two grating segments separated by a plain waveguide, referred to as spacer in this paper, constitutes a resonant cavity whose performance can be understood in analogy to a Fabry-Perot cavity. In

#137559 - $15.00 USD Received 2 Nov 2010; revised 11 Mar 2011; accepted 29 Mar 2011; published 8 Apr 2011

this case, however, the plane mirror reflectors of the Fabry-Perot cavity are replaced with distributed Bragg reflectors. Suppose the change of phase on reflection is φ_r at each spacer/grating interface, then the round-trip phase delay in the cavity can be described as $2\varphi_r + 2\beta_1 D$, where β_1 is the propagation constant in the spacer and D is the spacer length. If we choose a D that satisfies the phase condition of $2\varphi_r + 2\beta_1 D = 2\pi$, then a maximum transmittance can be achieved in this grating waveguide. On the other hand, since the grating waveguide transmittance depends on the choice of D, it is possible to obtain equal power transmission in both the reference T_r and modulation T_m arms ($T_r = T_m$) for discrete values of spacer lengths, D. If the spacer length for the modulation and reference arms are individually optimized, then the condition $T_r = T_m = 1$ can be achieved. In the case of multiple-segments ($M > 2$), several coupled cavities can be formed along the grating and we can follow the same procedure to determine the spacer length.

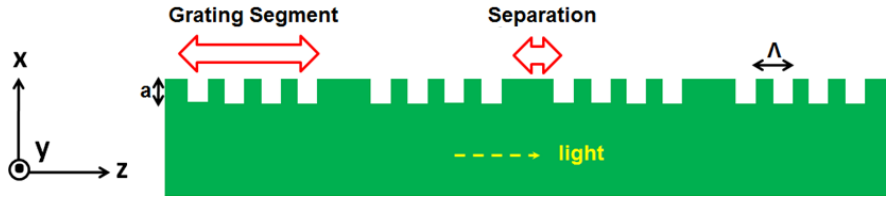

Fig. 6. Illustration of a multi-segment grating waveguide.

To analyze the performance of a multi-segment grating, we combine coupled-mode theory with complex transition matrices to describe the transmitted and reflected optical wave. These are similar to the transfer matrices representing a dielectric slab used when calculating transmission and reflection coefficients for a plane wave incident on a dielectric film slab. In our grating case, coupled-mode theory is used to obtain the transition matrix representing each segment. In subsection 5.1, transfer matrix construction is discussed in details. In subsection 5.2, 5.3 and 5.4, we summarize calculations for various multi-segment grating designs and discuss the results.

5.1 Matrix construction

To simplify the derivation process, we first calculate an auxiliary scattering matrix (S-matrix) and convert it to the corresponding transmission matrix (T-matrix). The S-matrix and T-matrix variables are defined in Fig. 7.

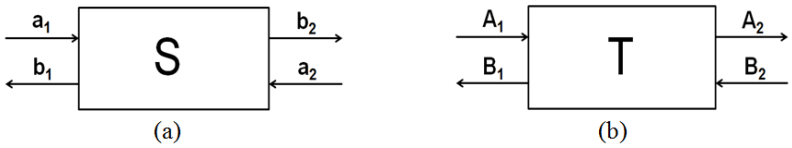

Fig. 7. (a) Scattering matrix (b) Transmission matrix.

If we compare the parameters defined in Fig. 1(c) with those in Fig. 7 (a), simple relations are established as follows: $a_1 = A(0)$, $a_2 = B(L)$, $b_1 = B(0)$, $b_2 = A(L)$. By using coupled-mode theory to calculate the complex amplitudes $A(0)$, $B(L)$, $B(0)$, and $A(L)$, the S-matrix parameters can be obtained as follows [18]:

#137559 - $15.00 USD Received 2 Nov 2010; revised 11 Mar 2011; accepted 29 Mar 2011; published 8 Apr 2011

$$\begin{cases} S_{11}=\dfrac{b_1}{a_1}\Big|_{a_2=0}=\dfrac{B(0)e^{i\frac{\pi}{\Lambda}0}}{A(0)e^{-i\frac{\pi}{\Lambda}0}}\Big|_{B(L)=0}=\dfrac{K^*\sinh(SL)}{-\Delta\beta\sinh(SL)+iS\cosh(SL)}, \\ S_{21}=\dfrac{b_2}{a_1}\Big|_{a_2=0}=\dfrac{A(L)e^{-i\frac{\pi}{\Lambda}L}}{A(0)e^{-i\frac{\pi}{\Lambda}0}}\Big|_{B(L)=0}=\dfrac{iS}{-\Delta\beta\sinh(SL)+iS\cosh(SL)}e^{-i\frac{\pi}{\Lambda}L}, \\ S_{22}=\dfrac{b_2}{a_2}\Big|_{a_1=0}=\dfrac{A(L)e^{-i\frac{\pi}{\Lambda}L}}{B(L)e^{i\frac{\pi}{\Lambda}L}}\Big|_{A(0)=0}=\dfrac{K\sinh(SL)}{-\Delta\beta\sinh(SL)+iS\cosh(SL)}e^{-i\frac{2\pi}{\Lambda}L}, \\ S_{12}=\dfrac{b_1}{a_2}\Big|_{a_1=0}=\dfrac{B(0)e^{i\frac{\pi}{\Lambda}0}}{B(L)e^{i\frac{\pi}{\Lambda}L}}\Big|_{A(0)=0}=\dfrac{iS}{-\Delta\beta\sinh(SL)+iS\cosh(SL)}e^{-i\frac{\pi}{\Lambda}L}. \end{cases} \tag{6}$$

The corresponding T-matrix of a grating segment (T_g) can be constructed by utilizing the following conversion relation:

$$T_g=\frac{1}{S_{21}}\begin{bmatrix}1 & -S_{22}\\ S_{11} & S_{12}S_{21}-S_{11}S_{22}\end{bmatrix}. \tag{7}$$

The T-matrix for a spacer (T_f) is as follows

$$T_f=\begin{bmatrix}e^{i\beta_s D} & 0\\ 0 & e^{-i\beta_s D}\end{bmatrix}. \tag{8}$$

With T_g and T_f calculated from Eq. (7) and (8), it is easy to calculate the total T-matrix for an M-segment configuration, the corresponding transmission coefficient t, and reflection coefficient r are obtained from Eqs. (9) and (10):

$$T=\underbrace{\left(T_gT_f\right)\left(T_gT_f\right)\cdots\left(T_gT_f\right)}_{(M-1)\text{ terms}}T_g, \tag{9}$$

$$r=\frac{T_{21}}{T_{11}}\quad\text{and}\quad t=\frac{1}{T_{11}}, \tag{10}$$

where T_{ij} are the matrix element of the transfer matrix T. The absolute value of the transmission coefficient t is termed the transmittance and is given by $|t|^2$. The phase change upon transmission is represented by $\tan^{-1}(t_{img}/t_{real})$, where t_{img} and t_{real} are the imaginary and real part of transmission coefficient, t.

5.2 M = 1,2,3 for fixed grating length

The length reduction ratio is taken to be 2.4, as an example for which the operating wavelength is λ = 1.574μm. At this wavelength, a group index of n_g = 14.9 is obtained from Fig. 3. For a single grating segment, M = 1, the grating length for π-phase shift is $L = 120\Lambda$. The calculated transmittance of the reference arm and modulation arm are T_r = 0.0516 and T_m = 0.3397, respectively. The small T_r and large difference $|T_r - T_m|$, gives rise to a high insertion loss (12.87dB) and low extinction ratio (−4.46dB).

In the multi-segment grating structure, we fix the grating length at 120Λ and plot T_r and T_m versus spacer length D. Figure 8 shows plots of T_r and T_m for a two-segment grating (M = 2) structure, where each grating segment has a length of 60Λ. The T_r and T_m curve in Fig. 8 shows periodicity of $D \approx 1.1\Lambda$. Since the total length of the grating structure is $L = 2 \times 60\Lambda + D$, a small spacer length is desirable for short MZI. We choose D between 0 and 1.1Λ.

#137559 - $15.00 USD Received 2 Nov 2010; revised 11 Mar 2011; accepted 29 Mar 2011; published 8 Apr 2011

Figure 8 shows two intersections at $D = 0.90\Lambda$ and at D = 0.97Λ. Of the two intersections, $D = 0.97\Lambda$ corresponds to a slightly higher transmittance, and is closer to π phase shift. The resulting parameters are $T_r = 0.2980$, $T_m = 0.2446$, and $\Delta\varphi = 0.933\pi$. $\Delta\varphi$ is the phase difference between the two arms calculated according to $\tan^{-1}(t_{img}/t_{real})$. The MZI insertion loss is 5.36dB and extinction ratio is 8.83dB. Here, the insertion loss is calculated as $10\log_{10}(T_r)$ and the extinction ratio is calculated as $10\log_{10}[2T_r/(T_r^2 + T_m^2 + 2T_rT_m\cos\Delta\varphi)^{1/2}]$. Following the same procedure, we evaluate an $M = 3$ grating waveguide. The best performance is achieved at $D = 0.98\Lambda$, which gives a total device length of $L = 3 \times 40\Lambda + 2 \times 0.98\Lambda$. In this case, calculations yield $T_r = 0.4790$, $T_m = 0.4411$, and $\Delta\varphi = 1.089\pi$, which corresponds to a loss of 3.20dB and an extinction ratio of 8.56dB. Compared to the $M = 2$ case, the $M = 3$ option yields a higher transmittance and thus a lower loss.

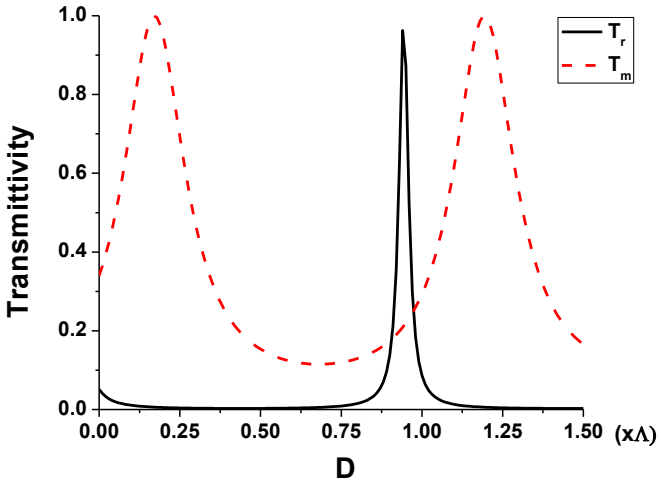

Fig. 8. T_r and T_m dependence on D for $M = 2$.

The above results indicate that the multi-segment grating waveguide results in a substantial performance improvement for both loss and extinction ratio. The insertion loss of the $M = 3$ design exhibits a loss reduction of 9.67dB, and an extinction ratio improvement of 13.29dB when compared to the MZI with a single grating segment and of approximately the same total length.

As shown in Fig. 8, T_r is *Lorentzian* function and always exhibits a single, narrow line shape whereas the T_m varies more gradually. Further investigation shows that T_m becomes even broader as L increases. Therefore, it is possible to manipulate the T_m curve to intercept the T_r curve at a higher transmittance point. Further discussion is presented in the following subsection.

5.3 M = 2,3 for unfixed grating length

In section 5.2, we demonstrated a performance enhancement attainable to a multi-segment grating waveguide with a fixed grating length of $L = 120\Lambda$. As discussed earlier, the transmittance of an $M = 2$ design can be evaluated simply by invoking F-P cavity theory in which the planar end-mirrors are replaced by a pair of distributed feed-back gratings. For a given grating segment length, the spacer length D determines the round trip phase delay $\delta = 2\varphi_r + 2\beta_1 D$ of the cavity. The transmittance of an F-P cavity is [19]

#137559 - $15.00 USD Received 2 Nov 2010; revised 11 Mar 2011; accepted 29 Mar 2011; published 8 Apr 2011

$$T_{m,r} = \frac{T_1^2}{1 + R_1^2 - 2R_1 \cos\delta}, \tag{11}$$

where T_1 and R_1 are the transmittance and reflectance at the grating/spacer interface and δ is the round trip phase shift for a plane wave of the F-P cavity. Energy conservation requires T_1 + R_1 = 1. Figure 9 plots the transmittance T_1 when the length of the grating segment changes from 0 to 80Λ. For the modulation arm, it is obvious that T_1 increases monotonically to 1 when the length of the grating segment increases from 60Λ to 80Λ. In other words, the reflectivity R_1 goes to 0, which makes the effect of δ negligible in Eq. (11). As a result, T_m approaches 1 regardless of the choice of D. For the M = 2 design, since each grating segment has a length of L/2, one segment change from 60Λ to 80Λ corresponds to a variation of total grating length from 120Λ to 160Λ. As for T_r, this changes very little, since T_1 in Eq. (11) is relatively insensitive to the length of the grating segment. However, because φ_r changes with grating segment length, the peak in a T_r vs. D plot will appear at different positions.

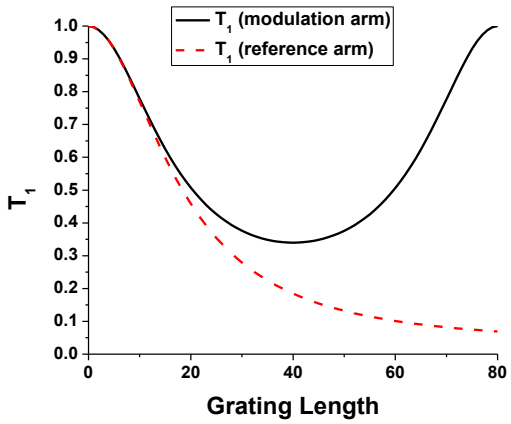

Fig. 9. T_1 verse grating length in the MZI.

We now explore the trade-off between grating segment length and the transmittance. As we increase the grating segment from 60Λ to 80Λ in the M = 2 design, i.e. a total length of approximately 160Λ, the T_m and T_r curves intersects at a point where the transmittance is high for both arms, as shown in Fig. 10. T_m is nearly a constant across a wide range of spacer lengths, D, as seen in Fig. 10 because it is insensitive to its phase delay δ, whereas T_r reaches its maximum when $\delta = 2\varphi_r + 2\beta_1 D = 2\pi$, i.e. the resonant condition of the F-P cavity. As the segment length varies, the spacer length D also varies to give rise to the maximum T_r. It is worth noting that L cannot be picked randomly from 120 Λ to 160Λ because the phase delay difference between the modulation and reference arm $\Delta\varphi$ needs to hold at π or close to π to obtain a good extinction ratio for the MZI.

#137559 - $15.00 USD Received 2 Nov 2010; revised 11 Mar 2011; accepted 29 Mar 2011; published 8 Apr 2011

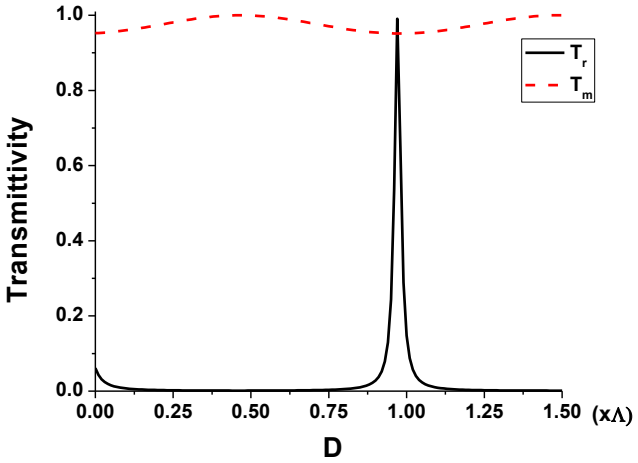

Fig. 10. T_r and T_m vs. D for $M = 2$ at $L = 156\Lambda$.

Our calculations show that for the $M = 2$ design, a grating length of 156Λ with $D = 0.97\Lambda$ gives $T_r = 0.9907$, $T_m = 0.9516$, and $\Delta\varphi = -0.9786\pi$, which correspond to a loss of 0.04dB and an extinction ratio of 14.16dB. Following the same argument and analysis, for the $M = 3$ design, a grating length of 140Λ with $D = 0.30\Lambda$ gives $T_r = 0.9616$, $T_m = 0.9630$, and $\Delta\varphi = 1.008\pi$. The corresponding loss is 0.17dB, and the extinction ratio is 18.84dB. The length reduction ratio is 1.84 and 2.06 for $M = 2$ and $M = 3$ design, respectively.

5.4 Unequal Ds for M = 2 design

In the discussion of section 5.2 where the size reduction ratio of 2.4 is fixed, we studied how the transmittance may vary with the spacer length D, which is the same for both the modulation and reference arms. In this subsection we propose and analyze the transmittance when the modulation and reference arms are optimized separately by varying D separately in order to achieve $T_m = T_r \approx 1$. We denote $D_{r,m}$ as the spacer length that gives the maximum transmittance for both T_r and T_m.

The adoption of different Ds could result in significant departure of $\Delta\varphi$ from π for a given length, which would degrade the extinction ratio of the MZI. The phase shift $\Delta\varphi$ consists of two parts: one is the phase difference caused by the light traveling in the cavity region, i.e. within the spacer; the other part arises from wave propagation in the grating segments. Within the cavity, due to separate optimization, both arms meet the phase condition for maximum transmittance. Therefore, the phase difference in the spacer between the two arms is zero. Our matrix calculations show that the phase difference due to a single grating segment is not proportional to the grating length. More specifically, in the case under study, the phase difference obtained from a grating segment of 60Λ is less than half that from a grating segment of 120Λ. Therefore, the total phase difference in the $M = 2$ configuration with two 60Λ segments is less than π, which is achieved in its $M = 1$ counterpart at $L = 120\Lambda$.

The $M = 2$ structure, for example, can be used to illustrate this idea. According to Fig. 8, the T_r and T_m reach their maximum value at $D_r = 0.94\Lambda$ and $D_m = 0.18\Lambda$, respectively. However, $\Delta\varphi$ is only 0.8463π, which limits the extinction ratio to 6.13dB. To improve $\Delta\varphi$ in this design, the grating length is allowed to extend at the expense of the reduction ratio, similar to the approach discussed in section 5.4.

As a summary, Table 1 below lists the designs and results from sections 5.2 to section 5.4.

#137559 - $15.00 USD Received 2 Nov 2010; revised 11 Mar 2011; accepted 29 Mar 2011; published 8 Apr 2011

Table 1. Summary of Different Multi-segment Designs

M	L	$\Delta\varphi$	T_r	T_m	D		Loss (dB)	ER (dB)
Fixed grating waveguide reduction ratio = 2.4								
1	120Λ	0.998π	0.0516	0.3397	-		12.87	–4.46
2	120Λ	–0.933π	0.2980	0.2446	0.97Λ		5.26	8.83
3	120Λ	1.0889π	0.4790	0.4411	0.98Λ		3.20	8.56
Extended grating waveguide length								
2	156Λ	–0.9786π	0.9907	0.9516	0.97Λ		0.04	14.16
3	140Λ	1.008π	0.9616	0.9630	0.30Λ		0.17	18.84
Different spacer length between the modulation and reference arm								
2	120Λ	0.8463π	0.9625	0.9944	D_r = 0.94Λ	D_m = 0.18Λ	0.17	6.13

6. Conclusion

In this paper, we have explored the slow light effect in a MZI structure consisting of 1D periodic gratings. The modeled structure consists of a slab silicon waveguide in a SiO_2/Si/SiO_2 structure in which the Si slab is 0.2mm thick and supports various grating structure on one surface. As an example, we have considered in details rectangular gratings with 30nm-deep grooves, subject to a refractive index change in the modulation arm of Δn = –0.01. We have demonstrated that this design gives a length reduction factor over 2 due to the slow light effects in the grating. To enhance the transmittance of the MZI in the slow light region, we have proposed a multi-segment grating design and have analyzed its performance by combining coupled-mode theory with a transfer matrix representation of the grating segments. A substantial reduction in the insertion loss and a substantial enhancement in the extinction ratio have been obtained. Tradeoffs between the reduction ratio, insertion loss and extinction ratio for different design variations are also presented in the paper. For a fixed reduction ratio of 2.4, we obtained a design with insertion loss of 0.17dB and extinction ratio of 6.13dB by matching the transmittance in the modulation arm and the reference arm. By trading reduction ratio for performance, an M = 3 design with a reduction ratio of 2.06 displays an insertion loss of 0.17dB and an extinction ratio of 18.84dB.

Acknowledgment

This research was supported in part by Nation Science Foundation (NSF) and in part by O'Brien & Gere. We also like to thank Dr. Daniel Guidotti for his many suggestions on the manuscript.

#137559 - $15.00 USD Received 2 Nov 2010; revised 11 Mar 2011; accepted 29 Mar 2011; published 8 Apr 2011